



Subscriber access provided by FLORIDA STATE UNIVERSITY LIBRARIES

Article

Theoretical and Experimental Insights Into Effects of Zn doping on Magnetic and Magnetocaloric Properties of MnCoGe

YiXu Wang, Vincent Yannello, Jacnel Graterol, Hu Zhang, Yi Long, and Michael Shatruk

Chem. Mater., Just Accepted Manuscript • DOI: 10.1021/acs.chemmater.0c02294 • Publication Date (Web): 10 Jul 2020

Downloaded from pubs.acs.org on July 26, 2020

Just Accepted

"Just Accepted" manuscripts have been peer-reviewed and accepted for publication. They are posted online prior to technical editing, formatting for publication and author proofing. The American Chemical Society provides "Just Accepted" as a service to the research community to expedite the dissemination of scientific material as soon as possible after acceptance. "Just Accepted" manuscripts appear in full in PDF format accompanied by an HTML abstract. "Just Accepted" manuscripts have been fully peer reviewed, but should not be considered the official version of record. They are citable by the Digital Object Identifier (DOI®). "Just Accepted" is an optional service offered to authors. Therefore, the "Just Accepted" Web site may not include all articles that will be published in the journal. After a manuscript is technically edited and formatted, it will be removed from the "Just Accepted" Web site and published as an ASAP article. Note that technical editing may introduce minor changes to the manuscript text and/or graphics which could affect content, and all legal disclaimers and ethical guidelines that apply to the journal pertain. ACS cannot be held responsible for errors or consequences arising from the use of information contained in these "Just Accepted" manuscripts.

Theoretical and Experimental Insights Into Effects of Zn doping on Magnetic and Magnetocaloric Properties of MnCoGe

YiXu Wang, a,b Vincent Yannello, b,† Jacnel Graterol, Hu Zhang, a,* Yi Long, Michael Shatrukb,c,*

- ^a School of Materials Science and Engineering, University of Science and Technology Beijing, Beijing, 100083, P. R. China
- ^b Department of Chemistry and Biochemistry, Florida State University, Tallahassee, Florida, 32306, United States
- ^c National High Magnetic Field Laboratory, Tallahassee, Florida, 32310, United States

ABSTRACT: MnCoGe-based materials have the potential to exhibit giant magnetocaloric effects due to coupling between magnetic ordering and a martensitic phase transition. Such coupling can be realized by matching the temperatures of the magnetic and structural phase transitions. To understand the site preference of different elements and the effect of hole or electron doping on the stability of different polymorphs of MnCoGe, crystal orbital Hamilton population (COHP) analysis has been employed for the first time to evaluate peculiarities of chemical bonding in this material. The shortest Mn–Mn bond in the structure is found to be pivotal to the observed ferromagnetic behavior and structural stability of hexagonal MnCoGe. Based on this insight, eliminating anti-bonding features of the shortest Mn–Mn bond at the Fermi energy is proposed as a feasible way to stabilize the hexagonal polymorph, which is then realized experimentally by substitution of Zn for Ge. The hexagonal MnCoGe structure is stabilized due to depopulation of the anti-bonding states and strengthening of the Mn–Mn bonding. This change in chemical bonding leads to anisotropic evolution of lattice parameters. The structural and magnetic properties of Zn-doped MnCoGe have been elucidated by synchrotron X-ray diffraction and magnetic measurements, respectively.

Introduction

Magnetic refrigerators based on the magnetocaloric effect (MCE) are appealing devices due to their high energy conversion efficiency and environmental friendliness.¹⁻² MnCoGe-based compounds represent a promising category of rare-earth-free magnetic refrigerants that have been studied extensively in recent years.3-4 Pristine MnCoGe exists as two polymorphs (Figure 1), a high-temperature hexagonal phase with the Ni₂In-type structure (h-MnCoGe, group $P6_3/mmc$) and a low-temperature orthorhombic phase with the TiNiSi-type structure (o-MnCoGe, space group *Pnma*). Both polymorphs can be described based on packing of face-sharing hexagonal prisms centered by Mn atoms, with the hexagonal faces being formed by alternating Co and Ge atoms (Figure 1). In *h*-MnCoGe, the prisms are stacked along the [001] direction. In the o-MnCoGe, the honeycomb Co/Ge layers are distorted. The relationship between the unit cells is described as $a_0 = c_h$, $b_0 = a_h$, and $c_0 = \sqrt{3}a_h$. Consequently, the linear rows of Mn atoms parallel to the [001] direction in h-MnCoGe are deformed into zigzag chains running along the [100] direction in *o*-MnCoGe. Another consequence of the orthorhombic symmetry lowering is the greater variability of interatomic distances in o-MnCoGe as compared to the distances in h-MnCoGe.

The structural phase transition (SPT) from h-MnCoGe to o-MnCoGe takes place at about 420 K, whereas ferromagnetic (FM) ordering in o-MnCoGe occurs at 355 K.⁵ This difference in temperature between the structural and magnetic transitions precludes the occurrence of a

potentially giant MCE in pristine MnCoGe and calls for chemical modifications aimed at coupling the two phase transitions.

Theoretically, the Curie temperature (T_c) of h-MnCoGe is found to be around 260 K.5 Of course, the SPT to the o-MnCoGe at 420 K prevents experimental verification of such prediction. It is anticipated that, once the structural phase transition temperature (T_{SPT}) can be lowered to approach the $T_{\rm C}$ value of o-MnCoGe, a giant MCE should be observed. The majority of attempts at such modifications have proceeded through a 'trial and error' approach. 6-14 Creation of vacancies and substitution of various chemical elements have been utilized to achieve the coupling between the magnetic and structural transitions. For example, Liu et al. managed to stabilize h-MnCoGe by creating Mn-vacancies (nominal composition $Mn_{1-x}CoGe$, 0.010 < x < 0.045), achieving a magnetic entropy change $(-\Delta S)$ as high as 26 J/kg K for a magnetic field change from 0 to 5 T around 290 K.5 In addition to creating vacancies, many elements have been probed as dopants in attempts to synchronize the magnetic and structural transitions in MnCoGe. Such doping has been applied to all three elements in the parent phase. The majority of these studies, however, have focused on substituting Mn or Co, while there have been relatively few efforts to modify the Ge site. For example, substituting Ga for Ge led to a first-order magnetostructural transition.8 The resulting material, MnCoGe_{0.95}Ga_{0.05}, showed a magnetic entropy change as high as ~34 J kg⁻¹ K⁻¹ around 318 K. On the contrary, no first-order magnetostructural transitions was observed for Cu-doped MnCoGe.⁶ The magnetic entropy change for $MnCoGe_{0.9}Cu_{0.1}$ was only 4.22 J kg⁻¹ K⁻¹ around 295 K. Zinc, an element intermediate between Ga and Cu, has not been probed as a substituent into the Ge site. Such substitution can shed light on the drastic difference between the effects caused by Ga and Cu doping, especially keeping in mind that Zn lies at the boundary between transition metals and post-transition elements.

Several theoretical papers reported total energy calculations and electron localization function (ELF)

analysis of *h*-MnCoGe and *o*-MnCoGe.¹⁵⁻¹⁷ It has been suggested that the valence electron concentration is a governing factor that defines the structural and magnetic behavior of these polymorphs.^{3, 5, 18-19} Nevertheless, a more explicit insight into correlations between the electronic structure and the phase stability and magnetism in MnCoGe is still lacking.

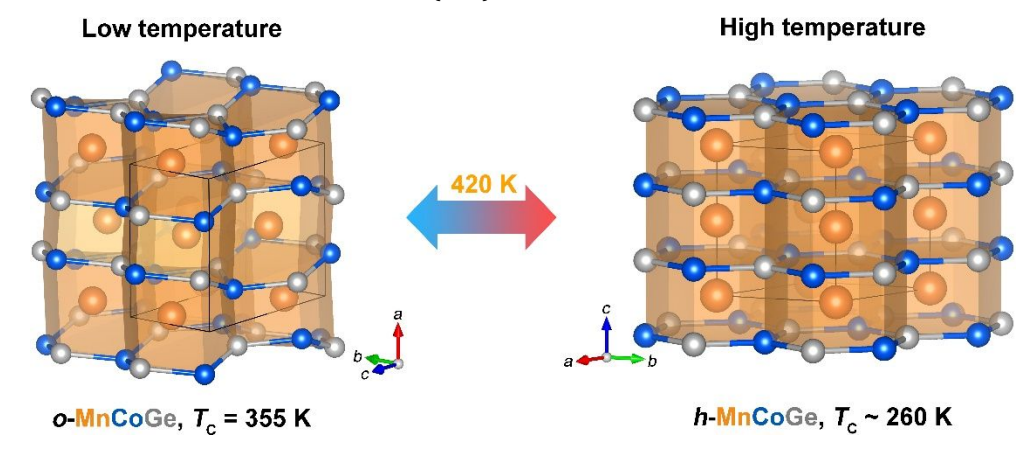


Figure 1. Orthorhombic (*o*) and hexagonal (*h*) polymorphs of MnCoGe. Color scheme: Mn = orange, Co = blue, Ge = gray.

Despite a wealth of efforts in this direction, several fundamental questions about this material remain open, including the site preference of transition metal atoms and the correlation between chemical bonding, structural stability, and magnetic properties. In this work, we use electronic structure calculations and crystal orbital Hamilton population (COHP) analysis to elucidate these relationships in h-MnCoGe. We follow upon the theoretical conclusions with an experimental study to probe effects of Zn for Ge substitution on the stability of *h*-MnCoGe. We then return to theory to interpret the experimental observations. Our theoretical findings suggest that the nearest-neighbor Mn-Mn interactions in h-MnCoGe have the most profound impact on the stability of the hexagonal polymorph. Both theoretical and experimental results demonstrate that the stability of this structure can be effectively tuned by minimizing anti-bonding contribution to the Mn-Mn interaction near the Fermi level, an effect that can be achieved by doping Zn into the Ge site of MnCoGe. These results offer a rational pathway for stabilizing the hexagonal structure of MnCoGe in order to couple the FM and structural phase transitions and achieve a giant MCE.

Materials and Methods

Synthesis. All sample preparation procedures were carried out in an argon-filled glove box (content of $O_2 < 0.1 \mathrm{ppm}$). Manganese pieces (99.98%, metal basis, Beantown) were first cleaned with dilute nitric acid (5 vol.%) and then pulverized by arc-melting and grinding the obtained ingot. Cobalt powder (99.998%, metal basis, Alfa Aesar) was purified by reduction at 773 K for 5 hours in a flow of H_2 gas. Germanium powder (99.999%, trace metal basis, Alfa Aesar) was used as received. A Zn button (99.999%, trace metal basis, Alfa Aesar) was first treated mechanically with a metal file to remove a dull ZnO layer and achieve metallic luster, after which the button was filed

to obtain Zn powder that was used without further purification. The samples with nominal compositions $MnCoGe_{1-x}Zn_x$ (x = 0, 0.02, 0.04, 0.05, 0.06, 0.08, 0.1) were synthesized by annealing stoichiometric mixtures of elements pressed into pellets of 8 mm diameter, with the total mass of each pellet ~300 mg. The pellets were sealed under dynamic vacuum (<10-5 Torr) in 10 mm inner diameter silica tubes, with the final length of the sealed tube ~50 mm. The pellets were heated to 1248 K at a rate of 5 K/min and maintained at that temperature for 12 h before being cooled down to room temperature by turning off the furnace. The tubes were opened in the glovebox, and the reaction mixtures were ground into fine powders and repelletized. The pellets were sealed again in evacuated silica tubes, annealed at 1248 K for 72 h, and cooled down to room temperature. The products were ground into fine powders and used for further measurements.

Powder X-ray Diffraction (PXRD) patterns were collected at room temperature using a high-resolution powder diffractometer at the synchrotron beamline 11-BM-B of the Advanced Photon Source at Argonne National Laboratory. Profile fitting and unit cell refinement were performed with FullProf.²⁰

Magnetic Measurements were performed with a SQUID MPMS-XL system (Quantum Design). Temperature dependence of magnetization was measured in the range from 5 to 400 K in an applied field of 0.01 T. Magnetization isotherms were recorded at multiple temperatures, from 40 K below to 40 K above the Curie temperature, with the magnetic field varying from 0 to 5 T.

Quantum-Mechanical Calculations. Density-functional theory (DFT) calculations were carried out using the Vienna Ab initio Simulation Package (VASP, version: 5.4.1).²¹⁻²² The projector augmented wave (PAW) pseudopotentials within the Perdew-Burke-Ernzerhof (PBE) generalized gradient approximation (GGA) of each

60

element were used in all calculations.²³ The following valence electron configurations of atoms were used: $3d^64s^1$ for Mn, $3d^84s^1$ for Co, $4s^24p^2$ for Ge, and $3d^{10}4s^2$ for Zn. The convergence criterion was set at 1×10⁻⁵ eV Å⁻¹. A Γcentered 17×17×13 Monkhorst-Pack k-point grid was chosen for sampling the first Brillouin zone of the hexagonal unit cell and an 8×13×7 mesh was used for the orthorhombic counterpart. In order to simulate the effects of doping, a 2×2×2 supercell of the *h*-MnCoGe structure and a 2×2×1 supercell of the o-MnCoGe structure were built starting from the parent unit cells that were optimized using non-spin-polarized (NSP) calculations. The k-point grids were scaled down according to the relationship between the unit cell and supercell, namely 9×9×7 for the hexagonal supercell and 4×7×7 for the orthorhombic supercell. In spin-polarized (SP) calculations, the starting magnetic moments of Mn and Co atoms were set to 5 μ_B per atom. First, geometry optimization of the models was carried out using the method of first-order Methfessel-Paxton with 0.2 eV as the width of smearing.²⁴ The atomic positions and the unit cell parameters and volume were optimized. After creating the supercells, the c/a ratio and unit cell volume were optimized for the hexagonal supercell, while only the volume was optimized for the orthorhombic supercell to prevent the atoms from moving off the idealized positions, since the substitution of a Zn atom for a Ge atom lowers the symmetry from orthorhombic to monoclinic. The optimized structures were used for self-consistent field (SCF) calculations in both NSP and SP models. The tetrahedron method with Blöchl corrections was employed for SCF calculations.²⁵ The COHP between specific atomic pairs²⁶ was calculated by using the Local-Orbital Basis Suite Towards Electronic-Structure Reconstruction (LOBSTER) code (version: 3.2.0).²⁷⁻²⁸

Results and Discussions

Electronic Structure Analysis. In the crystal structure of h-MnCoGe, each element occupies a distinct special position with fixed coordinates: Mn in 2a (0, 0, 0), Co in 2d(1/3, 2/3, 3/4), and Ge in 2c (1/3, 2/3, 1/4). Interestingly, the crystal structure refinement from neutron diffraction data showed only minor mixing between Mn and Co in the transition metal sites, with the Mn:Co ratio being 93:7 in the 2a site and 7:93 in the 2d site.²⁹ This strong site preference seems counter-intuitive, given the similar metallic radii of Mn and Co, which typically substitute for each other readily in many intermetallic compounds.³⁰⁻³³ We reasoned that the key to understanding the observed atomic distribution in h-MnCoGe lay in the electronic structure. Three models were used to simulate the switching of Mn and Co atoms in the 2a and 2d sites (Figure 2). In the "normal" model, the Mn and Co atoms occupy exclusively sites 2a and 2d, respectively, according to the experimental structure. The "mixed" model assumes statistical (50/50) mixing of Mn and Co atoms in both sites; creating such a model required lowering the space group symmetry from $P6_3/mmc$ to P3m1. The "inverse" model accounts for the complete reversal of the site occupancy.



Figure 2. Models for simulating different distributions of Mn and Co atoms in the crystal structure of *h*-MnCoGe. Color scheme: Mn = orange, Co = blue, Ge = gray.

Table 1. The total energies and unit cell parameters of the optimized structural models assuming different distributions of the Mn and Co atoms between the 2a and 2d sites of h-MnCoGe.

Structure	Model	Model E_{total} (eV/atom)		c (Å)
Normal	NSP	-6.817	4.065	4.924
Normai	SP	(eV/atom)	4.084	5.126
Mixture	NSP	-6.764	4.056	4.976
	SP	-6.882	4.115	4.987
Inverse	NSP	-6.697	4.096	4.892
	SP	-6.776	4.187	4.954
Experimental ²	N.A.	N.A.	4.067	5.284

Geometry optimizations were carried out for each structural model (the optimized structures are provided in the supporting information (SI) file, Tables S1-S6), and the SCF calculations were performed for both NSP and SP cases (Table 1). The calculations revealed that spin polarization always decreases the total energy of the system, indicating the tendency toward magnetic ordering in all three models. (The difference in the total energies is substantially above the calculation error of ~ 1 meV/atom.) Furthermore, among the SP models, the normal structure possesses the lowest total energy and shows the unit cell parameters most similar to those found in the experimentally determined crystal structure.²⁹ These results, however, do not elucidate explicitly the reasons behind the preferred atomic site distribution in the structure of h-MnCoGe.

COHP analysis was used to investigate the changes in chemical bonding that accompany the variation of atomic distributions in h-MnCoGe. As bonding between the constituent atoms becomes rather weak at distances above 3 Å, calculations focused only at pairwise interactions that occur below this limiting value. Results of such calculations on the normal NSP structure of h-MnCoGe are plotted in Figure 3, where the positive and negative regions of the -COHP function indicate, respectively, bonding and antibonding interactions, while the values near zero indicate nonbonding interactions. The Fermi level $(E_{\rm F})$ passes through a pronounced antibonding peak for the Mn-Mn, Mn-Co, and Mn-Ge interactions. The occurrence of anti-bonding peaks at $E_{\rm F}$ increases the total energy and destabilizes the structure.34-35 A way out of this instability is spin polarization that leads to the spontaneous magnetic ordering. The decrease in the energy of the majority-spin states and the increase in the energy of the minority-spin states reduces the antibonding character at $E_{\rm F}$, thus stabilizing the structure, as long as such stabilization is justified by the extent of energy gain due to the magnetic exchange and magnetic ordering below $T_{\rm C}$. This conclusion also agrees with the previous experimental works that attributed the magnetic ordering in MnCoGebased compounds to the exchange interactions between the nearest-neighbor Mn atoms. 8,38

We should also note that, among all bonds analyzed in the normal h-MnCoGe structure, only the shortest Co-Ge contact (referred to as Co-Ge_1) shows a peak that corresponds to bonding states at $E_{\rm F}$. This finding is in agreement with the recent theoretical report, which suggested that the covalent-like bonds between the nearest-neighbor Co and Ge atoms (i.e., the Co-Ge_1 interaction) provide stability to the hexagonal structure.³⁹

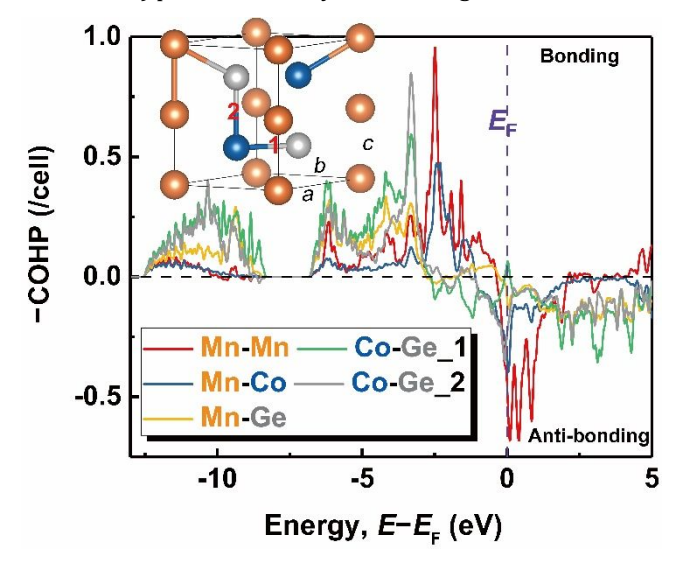


Figure 3. COHP curves calculated for selected interatomic contacts in the normal non-spin-polarized structure of *h*-MnCoGe. Inset: the model and interactions evaluated by the calculations. Color scheme: Mn = orange, Co = blue, Ge = gray.

Similar COHP analysis was also performed for the mixed and inverse structural models, in order to observe the evolution of bonding as a function of transition metal distribution over the 2a and 2d sites. In the normal structure, the Mn-Mn interactions are strongly antibonding at the Fermi level. Switching Mn and Co atoms is equivalent to adding electrons to the formerly Mn-Mn and Mn-Ge bonds and removing electrons from the Co-Ge bonds, while the number of electrons in the Mn-Co bonds remains the same. The –COHP plot (Figure 3) suggests that this change should lead to further population of the strongly antibonding states seen for the Mn-Mn interactions in the normal structure.

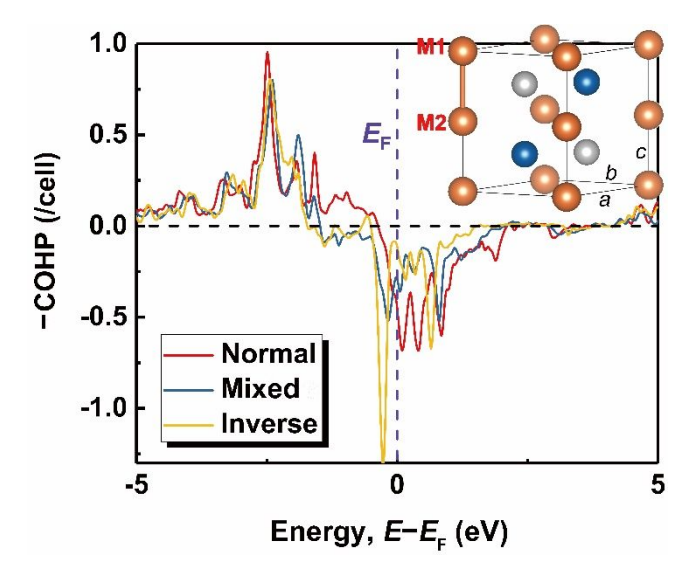


Figure 4. The COHP curves of the M1-M2 interaction calculated for three different structural models of *h*-MnCoGe. The inset shows the general structural model, emphasizing the M1-M2 bond.

Table 2. The bond length and –ICOHP values for the M1-M2 interaction calculated for different structural models of *h*-MnCoGe.

Structure	M1-M2 Distance (Å)	-ICOHP (eV/bond)
Normal	2.462	1.02
Mixture	2.488	0.65
Inverse	2.446	0.58

The COHP curves of the nearest Mn-Mn bond in the normal structure and its equivalents in the mixed and inverse structures, hereafter labeled as the M1-M2 bond, are compared in Figure 4. As expected, switching the Mn and Co atoms in the h-MnCoGe structure leads to the increase in the population of anti-bonding states for the M1-M2 interaction, justifying the increase in the total energy (Table 1). Integrating the -COHP curves up to the Fermi level provides the integral COHP (-ICOHP) values, which qualitatively correlate with the strength of corresponding bonds (Table 2). As can be seen, the M1-M2 bond strength is significantly reduced once the Mn and Co atoms are switched. It was reported that the strength of this bond correlates with the stability of the h-MnCoGe structure.8, 40 populating antibonding M1-M2 Therefore, states destabilizes the structure. To optimize the structural stability, Mn and Co atoms show strong preference to occupy the 2a and 2d sites, respectively.

As the result of the diffusionless structural transition from h-MnCoGe to o-MnCoGe, 41 the orthorhombic structure inherits, to a considerable extent, the physical and chemical characteristics of the hexagonal structure. From a crystallographic point of view, the nearest Mn-Mn contact in o-MnCoGe emerges directly from the M1-M2 bond in h-MnCoGe. It has already been shown that the nearest Mn-Mn interaction in o-MnCoGe is dominant in defining the magnetic behavior, similar to the importance of the M1-M2 bond in h-MnCoGe. 38 , 42 In the same vein, the distinct site preference observed for the Mn and Co atoms in the h-

MnCoGe structure can be also expected in the o-MnCoGe structure. In the latter, the Mn, Co, and Ge atoms occupy 4c positions (x,1/4,z) of the Pnma space group, differing only in the x and z values. ⁴³ In comparison to h-MnCoGe, however, o-MnCoGe has a more complex structure, with twice as many unique atoms, which makes the site preference analysis much more difficult. While the NSP geometry optimization of o-MnCoGe converged successfully (Table S7), attempts to optimize the geometry in the SP regime tended to push the atoms toward the hexagonal symmetry (Table S8), which is likely an artifact of the calculations. Thus, in further elucidation of relationships between the properties and chemical bonding, we will focus only on the hexagonal structure, for which such relationships can be analyzed more meaningfully.

Stabilizing *h***-MnCoGe via Hole Doping.** The analysis of the M1-M2 bonding suggests a way to stabilize the h-MnCoGe structure. The anti-bonding interactions observed at the Fermi level are electronically unfavorable. Decreasing the valence electron count in the system should lower the population of anti-bonding states and stabilize h-MnCoGe. Such minor hole doping should not cause a drastic reconstruction of the electronic structure. We chose to decrease the electron count in MnCoGe by substituting a pelement with fewer valence electrons for Ge. As discussed in the Introduction, such substitutions with Ga and Cu have been already reported. The Ga doping was found to synchronize the magnetic and structural transitions in $MnCoGe_{1-x}Ga_x$ at an appropriate value of x,8 while the Cu doping failed to induce a first-order magnetostructural transition.⁶ Therefore, we chose to dope MnCoGe with Zn, the element between Cu and Ga, to fill this experimental gap.

Samples with nominal compositions $MnCoGe_{1-x}Zn_x$ (x=0.02, 0.04, 0.05, 0.06, 0.08 and 0.1) were synthesized and found to contain only MnCoGe-based phases by room-temperature PXRD analysis. A clear transition from pure o-MnCoGe to a mixture of o-MnCoGe and h-MnCoGe phases at x=0.02 to pure h-MnCoGe at $x\geq 0.04$ was observed (Figure 5a). Interestingly, the lattice parameters of the Zn-doped samples remained almost unchanged with increasing Zn content (Figure 5b), despite the larger metallic radius of Zn as compared to that of Ge. These observations suggest there is an additional factor that affects the unit cell volume and counteracts the expected expansion caused by Zn doping. Theoretical analysis was performed again in order to understand the observed behavior.

To simulate the doping with a small amount of Zn, a $2\times2\times2$ supercell of h-MnCoGe and a $2\times2\times1$ supercell of o-MnCoGe were constructed, and one of the symmetry-independent Ge atoms in each structure was replaced with a Zn atom (Figures S1a and S1b). Such models correspond to a composition with x = 0.0625. The geometry of each supercell was optimized (Tables S9-S12), and the total energy values were calculated (Table 3). The total energy calculations of pure (undoped) MnCoGe are also shown for comparison.

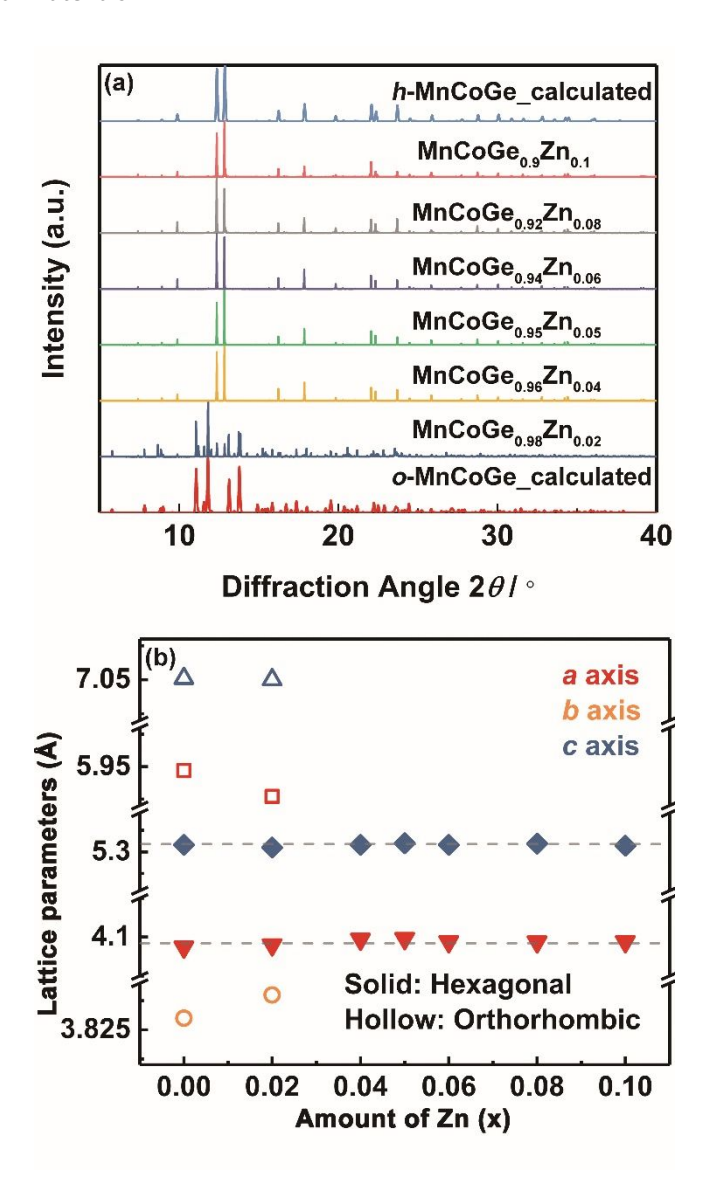


Figure 5. (a) Synchrotron PXRD data of MnCoGe_{1-x}Zn_x (x = 0.02, 0.04, 0.05, 0.06, 0.08, 0.1) and (b) lattice parameters of h-MnCoGe and o-MnCoGe as a function of Zn content.

In the case of pure MnCoGe, the orthorhombic polymorph is energetically favorable, regardless of spin-polarization and in agreement with the experimental observations that show the strong preference for o-MnCoGe as the temperature is decreased. The difference in the total energy of the two polymorphs, $\Delta E_{\rm str}$, calculated for the SP case, is close to the reported experimental value, 15 which thus supports the reliability of our calculations. Upon Zn doping, the $\Delta E_{\rm str}$ value decreases for both NSP and SP calculations, although less dramatically in the latter case. Nevertheless, the change in the sign of $\Delta E_{\rm str}$ suggests that Zn doping should stabilize the h-MnCoGe structure, in agreement with our experimental observations (Figure 5). It is worth noting that the error of total energy calculations is ~ 1 meV/atom. Thus, it is difficult to draw a clear conclusion that h-MnCoGe becomes more stable than o-MnCoGe in the SP calculations. but the trend toward stabilization of the hexagonal polymorph via Zn doping is clear.

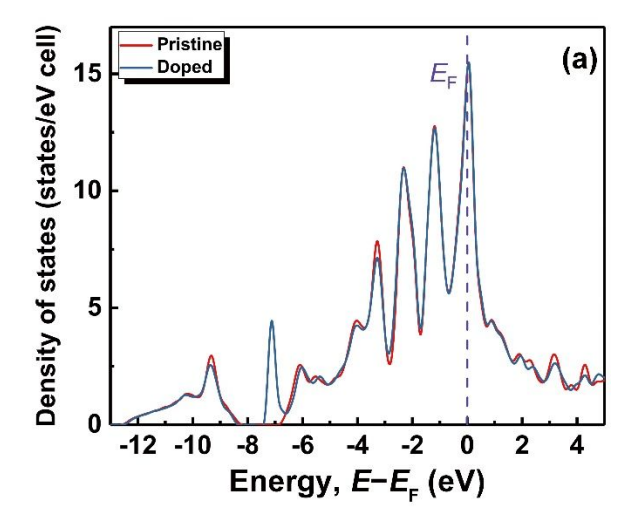
Table 3. Total energies of pure and Zn-doped structures for both h-MnCoGe and o-MnCoGe. The total energy difference between the two polymorphs is given as $\Delta E_{\text{str}} = E_h - E_o$.

	h-MnCoGe		o-MnCoGe		$\Delta E_{ m str}$	
Calcs.	(eV/atom)		(eV/atom)		(meV/atom)	
Type	Pure	Doped	Pure	Doped	Pur	Doped
					e	
NSP	-6.817	-6.730	-6.850	-6.676	33	-54
SP	-7.022	-6.936	-7.030	-6.935	8	-1

Figure 6a displays the total DOS of h-MnCoGe for the pure and doped structures. The changes stemming from Zn doping are very subtle. The three well-defined peaks close to the Fermi level remain almost unaffected. The appearance of a DOS peak near -7 eV can be attributed to d-states of Zn, while the slight decrease in the DOS values near -9.5 eV and -3.5 eV is due to the decrease in the concentration of Ge p-electrons in the doped structure. (Note that the d-states of Ge have been treated as a core and, thus, not explicitly included in the calculations.)

The COHP curves for the M1-M2 bond were calculated to check the influence of Zn doping on the anti-bonding states near the Fermi level. To account for the effect of mixed occupancy of the 2c site by Zn and Ge atoms, the COHP plot was averaged over all sixteen bonds in the supercell that are identical to the M1-M2 bond in the parent unit cell. As can be seen from Figure 6b (and more details in Figure S2-S6), the substitution of Zn for Ge has a rather minor effect on the |-COHP| values for the M1-M2 contacts. Nevertheless, the anti-bonding character of these interactions just below the Fermi level is significantly reduced (Figure 6b, inset), justifying the increased stability of h-MnCoGe upon Zn doping. A numerical evidence for the reduced anti-bonding states is provided by the decrease in the calculated bond lengths and increase in the -ICOHP values (Table 4), both in agreement with the stronger M1-M2 bonds.

To analyze the changes in interatomic distances, the calculated bond lengths and corresponding -ICOHP values for h-MnCoGe are summarized in Table 5. As shown in Figure 1, this crystal structure can be viewed as a packing of Mn-centered hexagonal prisms having alternating Co and Ge atoms in the vertices. The Co-Ge_1 bonds form the hexagonal faces of the prisms in the ab plane while the Co-Ge_2 bonds form the lateral edges parallel to the c axis. With Zn doping, the M1-M2 and Co-Ge_2 bonds contract, the Co-Ge_1 bonds expand, and the Mn-Co and Mn-Ge bonds remain intact. The a parameter correlates with the Co-Ge_1 bond: $a = \sqrt{3} \times d(\text{Co-Ge_1})$, while the *c* parameter is a double of the M1-M2 and Co-Ge_2 bond lengths. The changes in these bonds explain the elongation of the a axis and the shrinkage of the c axis caused by Zn doping, although the effect is rather small, as can be seen from only ~0.12% change in the unit cell volume calculated for the pure and doped structures under spin-polarized conditions. This observation is consistent with the negligible changes in the unit cell parameters of h-MnCoGe upon Zn doping (Figure 5b). Note that in the case of vacancy formation in the Ge site, a much more significant decrease in the unit cell volume has been reported.44



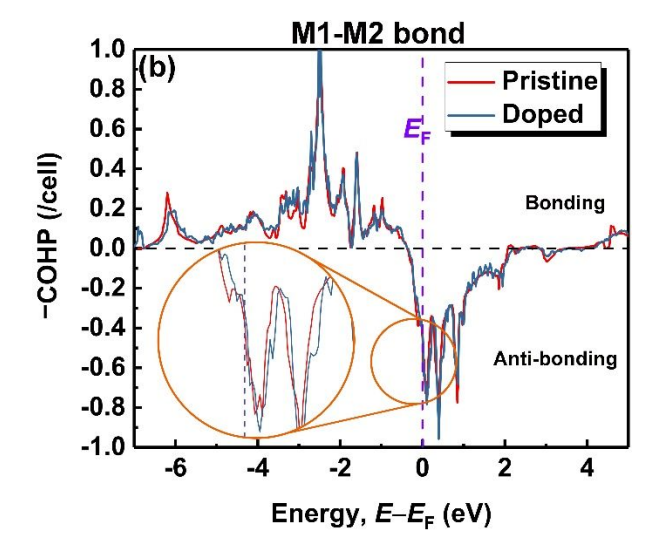


Figure 6. A comparison of the total density of states (a) and COHP curves for the M1-M2 bond (b) in the pristine and doped structures of *h*-MnCoGe. The inset shows the zoomed-in figure of a selected region of COHP curves.

Table 4. The unit cell parameters, volume, M1-M2 bond length, and –ICOHP values calculated for pure and doped *h*-MnCoGe. In the case of SP calculations, the –ICOHP values are shown for the spin-up and spin-down channels, and the total bond strength should correlate with the sum of those two numbers.

	Calcs. a (Å) c (Å)	17 (Å 3)	d(M1-M2)	-ICOHP		
	Type	Calcs. Type a (Å) c (Å) V (ų)	V (A°)	(Å)	(eV/bond)	
Duna	NSP	4.065	4.924	70.464	2.462	1.01
Pure	SP	4.084	5.126	74.042	2.563	0.23/0.48
Doped	NSP	4.072	4.900	70.363	2.450	1.06
	SP	4.088	5.110	73.956	2.555	0.25/0.50

Table 5. The calculated bond lengths and corresponding – ICOHP values (in parentheses) in MnCoGe and MnCoGe $_{0.9375}$ Zn $_{0.0625}$. In the case of SP calculations, the –ICOHP values are shown for the spin-up and spin-down channels, and the total bond strength should correlate with the sum of those two numbers.

Type -		Pure	Doped		
Type .	NSP	SP	NSP	SP	
M1-M2	2.462	2.563	2.451	2.555	
	(1.01)	(0.23/0.48)	(1.06)	(0.24/0.49)	
Mn-Co	2.650	2.684	2.652	2.684	
	(0.50)	(0.17/0.29)	(0.50)	(0.17/0.30)	
Mn-Ge	2.650	2.684	2.652	2.684	
	(1.11)	(0.48/0.53)	(1.05)	(0.45/0.50)	
Co-Ge_1	2.347	2.358	2.352	2.360	
	(1.61)	(0.83/0.83)	(1.48)	(0.77/0.77)	
Co-Ge_2	2.462	2.563	2.451	2.555	
	(1.22)	(0.52/0.54)	(1.20)	(0.50/0.53)	

Magnetic Properties and Magnetocaloric Effect of Zn-doped MnCoGe. Magnetic measurements were performed on powder samples of $MnCoGe_{1-x}Zn_x$ with x=0, 0.02, 0.04, and 0.05, according to the doping region across which the stabilization of the h-MnCoGe structure was observed in the PXRD data. The field-cooled (FC) and zero-field-cooled (ZFC) magnetization measurements revealed a decrease in the FM ordering temperature (T_C) and the occurrence and disappearance of magnetic hysteresis with the increasing Zn content (Figure 7a). In the undoped MnCoGe, the structural and magnetic phase transitions are decoupled. Therefore, the FM ordering is a second-order non-hysteretic transition.

At x = 0.02, the coupling of the SPT and FM ordering results in the thermal hysteresis that is consistent with the observation of two phases in the PXRD pattern of this sample. At x = 0.04, a small thermal hysteresis is still observed but its occurrence indicates that T_{SPT} had been suppressed below room temperature. For this sample, the value of T_{SPT} has been shifted to the lower limit of the T_C window and, thus, decoupling of the SPT and FM ordering is expected at higher Zn content. Indeed, two separate transitions were observed for the sample with x = 0.05. The reversible transition near 260 K represents the FM ordering of h-MnCoGe while the transition near 220 K corresponds to the SPT from *h*-MnCoGe to *o*-MnCoGe. The complex behavior of the MnCoGe_{0.95}Zn_{0.05} sample signifies that the SPT has been shifted too far in temperature, taking place below the Curie temperature of *h*-MnCoGe.

The MCE of the sample with x=0.02 was evaluated from the magnetization isotherms measured across the FM transition region (Figure S7). The magnetic entropy change $(\Delta S_{\rm M})$ was calculated from the Maxwell relation:

$$\Delta S_{\rm M} = \mu_0 \int_0^H \frac{\partial M}{\partial T} dH \tag{2}$$

where μ_0 , M, T, and H are the magnetic permeability constant, magnetization, temperature, and magnetic field, respectively. The variation in $\Delta S_{\rm M}$ as a function of temperature is shown in Figure 7b. Despite the expectation of giant MCE in MnCoGe_{0.98}Zn_{0.02}, the maximum $\Delta S_{\rm M}$, observed under magnetic field change of 5 T, was only \sim 6.5

J kg⁻¹ K⁻¹, which is substantially lower than the values observed for MnCoGe_{0.95}Ga_{0.05} (\sim 34 J kg⁻¹ K⁻¹, from a first-order magnetostructural transition) but higher than the entropy change found for MnCoGe_{0.9}Cu_{0.1} (4.23 J kg⁻¹ K⁻¹, from a second-order magnetic transition). The lower $\Delta S_{\rm M}$ value might be explained by a plateau-like region observed in the $\Delta S_{\rm M}$ vs. T curves, which hints at compositional inhomogeneity of the sample.

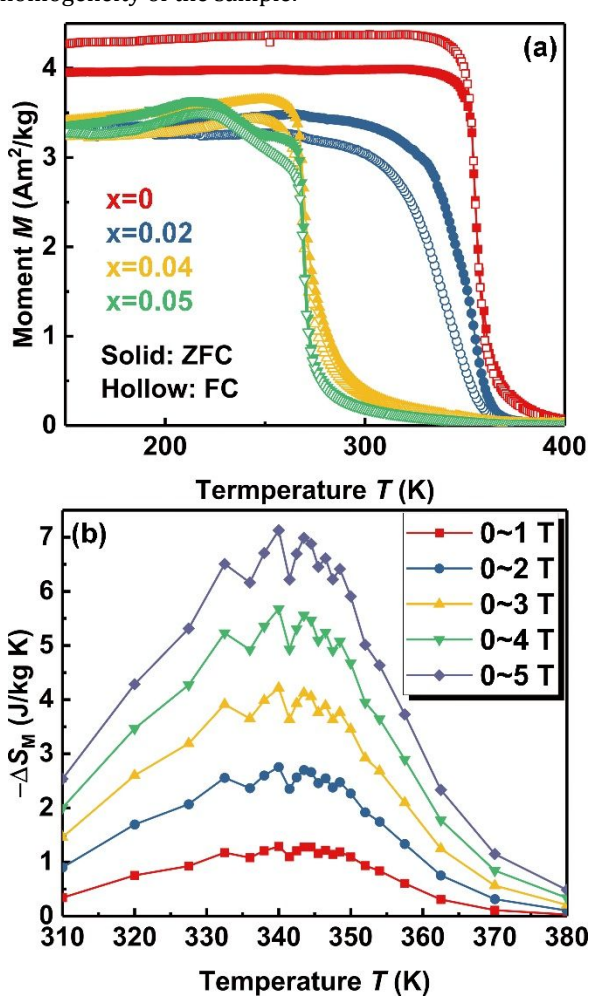


Figure 7. (a) The temperature dependence of field-cooled and zero-field-cooled magnetization for MnCoGe_{1-x}Zn_x (x = 0, 0.02, 0.04, 0.05) and (b) the variation of magnetic entropy change of MnCoGe_{0.98}Zn_{0.02} as a function of temperature under different changes in the applied magnetic field.

To prove that the FM transition is of the first-order, the $\Delta S_{\rm M}$ -T curves were reconstructed to extract the exponent n of the equation

$$\Delta S_{\rm M} \propto H^n$$
 (3)

where n was calculated by using 45 $n(T,H) = \frac{\mathrm{dln}|\Delta S_{\mathrm{M}}|}{\mathrm{dln}H}$

$$n(T,H) = \frac{\mathrm{dln}|\Delta S_M|}{\mathrm{dln}H} \tag{4}$$

The calculated n values are plotted in Figure S8. After the reconstruction of the $\Delta S_{\rm M}$ -T curves, the temperature and field dependent magnetic entropy changes are rescaled. A highly overlapping area can be observed between 340 K and 350 K, corresponding to the plateaus in the $\Delta S_{\rm M}$ -T curves. The value of n is very close to 1 in this region, which is in accord with features of first-order phase transitions

reported previously for various magnetocaloric materials. $^{46-49}$ Additionally, the plateau region seen in the n-T curve also indicates that the sample might be compositionally inhomogeneous. Such inhomogeneity should lead to a spread in the magnetostructural transition temperature, manifesting itself as a series of highly overlapping peaks that result in the plateau regions in the $\Delta S_{\rm M}$ -T and n-T curves.

Conclusions

In summary, we have provided a theoretical insight to facilitate the chemical understandings of magnetostructural coupling than impacts the magnetocaloric effect in MnCoGe-based materials. The distinct site preference of Mn and Co atoms in the h-MnCoGe structure becomes understandable from the chemical bonding perspective provided by the COHP analysis. Mixing Co atoms into the Mn site results in population of anti-bonding states of M1-M2 bonds, thus increasing the total energy of the system and destabilizing the structure. An experimental way to stabilize the *h*-MnCoGe phase is to decrease the valence electron count, which was pursued by doping Zn into Ge sites. Such doping, however, led to a counter-intuitive evolution of the crystal structure parameters, which was subsequently understood via electronic structure calculations that showed strengthening of the M1-M2 bond caused by Zn Finally, the magnetic properties magnetocaloric effect in Zn-doped MnCoGe samples reveal the first-order nature of the phase transition in $MnCoGe_{0.98}Zn_{0.02}$, as demonstrated by the analysis of the nexponent in the field dependence of magnetic entropy change.

ASSOCIATED CONTENT

Supporting Information. Results of geometry optimization results for all crystal structures. The $2 \times 2 \times 2$ supercell of h-MnCoGe and a $2 \times 2 \times 1$ supercell of o-MnCoGe, COHP curves of predominant bonds in h-MnCoGe after Zn doping and the comparisons of them with the ones in pure h-MnCoGe. This material is available free of charge via the Internet at http://pubs.acs.org.

AUTHOR INFORMATION

Corresponding Authors

Michael Shatruk: mshatruk@fsu.edu Hu Zhang: zhanghu@ustb.edu.cn

Present Addresses

† 401 W Kennedy Blvd, Tampa, FL 33606, United States

Author Contributions

Y.X.W. and V.Y. carried out theoretical studies. Y.X.W. and J.G. performed experimental synthesis and magnetic measurements. H.Z. and M.S. supervised the project and participated in the analysis and discussion of the results. Y.X.W., H.Z., Y.L., and M.S. co-wrote the manuscript.

Funding Sources

This work was supported by the National Natural Science Foundation of China (Grant No.: 51671022); the National Key Research and Development Program of China (Grant No.: 2017YFB0702704); the State Key Lab of Advanced Metals and

Materials (Grant No. 2019-Z11); Beijing Natural Science Foundation (No. 2182006); and the Fundamental Research Funds for the Central Universities (Grant No.: FRF-TP-18-014B1). M.S. and V.Y. acknowledge support by the National Science Foundation (award DMR-1905499). Y. X. W. acknowledges the Chinese Scholarship Council for supporting his visit to Florida State University (No. 201706460046). Use of the Advanced Photon Source at Argonne National Laboratory was supported by the U. S. Department of Energy, Office of Science, Office of Basic Energy Sciences, under Contract No. DE-AC02-06CH11357.

ABBREVIATIONS

COHP crystal orbital Hamilton population; DFT density functional theory; DOS density of states; FM ferromagnetic; ICOHP integral crystal orbital Hamilton population; PXRD powder X-ray diffraction.

REFERENCES

- 1. Moya, X.; Defay, E.; Heine, V.; Mathur, N. D. Too cool to work. *Nat. Phys.* **2015**, *11*, 202-205.
- Moya, X.; Kar-Narayan, S.; Mathur, N. D. Caloric materials near ferroic phase transitions. *Nat. Mater.* 2014, 13, 439-450.
- Ren, Q.; Hutchison, W. D.; Wang, J.; Studer, A. J.; Campbell, S. J. Magnetic and structural transitions tuned through valence electron concentration in magnetocaloric Mn(Co_{1-x}Ni_x)Ge. *Chem. Mater.* 2018, *30*, 1324-1334.
- Aznar, A.; Lloveras, P.; Kim, J.-Y.; Stern-Taulats, E.; Barrio, M.; Tamarit, J. L.; Sánchez-Valdés, C. F.; Sánchez Llamazares, J. L.; Mathur, N. D.; Moya, X. Giant and reversible inverse barocaloric effects near room temperature in ferromagnetic MnCoGeB_{0.03}. Adv. Mater. 2019, 31, 1903577.
- Liu, E. K.; Zhu, W.; Feng, L.; Chen, J. L.; Wang, W. H.; Wu, G. H.; Liu, H. Y.; Meng, F. B.; Luo, H. Z.; Li, Y. X. Vacancy-tuned paramagnetic/ferromagnetic martensitic transformation in Mn-poor Mn_{1-x}CoGe alloys. *Europhys. Lett.* 2010, *91*, 17003.
- Shen, Y.; Liu, Y.; Yu, W.; Ma, X.; Zhang, Z.; Lin, J.; Luo, X. Large room-temperature magnetocaloric effect in MnCoGe_{0.9}Cu_{0.1} alloy. *Mater. Res. Express* 2017, 4, 116110.
- Guillou, F.; Wilhelm, F.; Tegus, O.; Rogalev, A. Microscopic mechanism of the giant magnetocaloric effect in MnCoGe alloys probed by x-ray magnetic circular dichroism. *Appl. Phys. Lett.* 2016, 108, 122405.
- 8. Zhang, D.; Nie, Z.; Wang, Z.; Huang, L.; Zhang, Q.; Wang, Y.-d. Giant magnetocaloric effect in MnCoGe with minimal Ga substitution. *J. Magn. Magn. Mater.* **2015**, *387*, 107-110.
- Liu, Y.; Shen, F. R.; Zhang, M.; Bao, L. F.; Wu, R. R.; Zhao, Y. Y.; Hu, F. X.; Wang, J.; Zuo, W. L.; Sun, J. R.; Shen, B. G. Stress modulated martensitic transition and magnetocaloric effect in hexagonal Ni₂In-type MnCoGe_{1-x}In_x alloys. *J. Alloys* Compd. 2015, 649, 1048-1052.
- Lai, J. W.; Zheng, Z. G.; Montemayor, R.; Zhong, X. C.; Liu, Z. W.; Zeng, D. C. Magnetic phase transitions and magnetocaloric effect of MnCoGe_{1-x}Si_x. *J. Magn. Magn. Mater.* 2014, 372, 86-90.
- 11. Bao, L. F.; Hu, F. X.; Wu, R. R.; Wang, J.; Chen, L.; Sun, J. R.; Shen, B. G.; Li, L.; Zhang, B.; Zhang, X. X. Evolution of magnetostructural transition and magnetocaloric effect with Al doping in MnCoGe_{1-x}Al_x compounds. *J. Phys. D* 2014, 47, 055003.
- 12. Pal, S. K.; Frommen, C.; Kumar, S.; Hauback, B. C.; Fjellvåg, H.; Woodcock, T. G.; Nielsch, K.; Helgesen, G. Comparative phase transformation and magnetocaloric effect study of Co

60

- and Mn substitution by Cu in MnCoGe compounds. *J. Alloys Compd.* **2019**, *775*, 22-29.
- Devarajan, U.; Nair, S. Investigations on Cu induced coupledecoupled magneto-structural transition in MnCoGe alloys. *Mater. Res. Express* 2019, 6, 106117.
- 14. Zhang, C. L.; Nie, Y. G.; Shi, H. F.; Ye, E. J.; Zhao, J. Q.; Han, Z. D.; Xuan, H. C.; Wang, D. H. Tunable magnetostructural coupling and large magnetocaloric effect in Mn_{1-x}Ni_{1-x}Fe_{2x}Si_{1-x}Ga_x. J. Magn. Magn. Mater. 2017, 432, 527-531.
- 15. Hahn, K. R.; Assaf, E.; Portavoce, A.; Bertaina, S.; Charaï, A. Structural and composition effects on electronic and magnetic properties in thermoelectric $Mn_{1-x-y}Co_{1+x}Ge_{1+y}$ materials. *J. Phys. Chem. C* **2017**, *121*, 26575-26586.
- Biswas, A.; Pathak, A. K.; Zarkevich, N. A.; Liu, X.; Mudryk, Y.; Balema, V.; Johnson, D. D.; Pecharsky, V. K. Designed materials with the giant magnetocaloric effect near room temperature. *Acta Mater.* 2019, *180*, 341-348.
- 17. Kaprzyk, S.; Niziol, S. The electronic structure of CoMnGe with the hexagonal and orthorhombic crystal structure. *J. Magn. Magn. Mater.* **1990**, *87*, 267-275.
- 18. Liu, E.; Wang, W.; Feng, L.; Zhu, W.; Li, G.; Chen, J.; Zhang, H.; Wu, G.; Jiang, C.; Xu, H.; de Boer, F. Stable magnetostructural coupling with tunable magnetoresponsive effects in hexagonal ferromagnets. *Nat. Commun.* **2012**, *3*, 873.
- 19. Tozkoparan, O.; Yildirim, O.; Yüzüak, E.; Duman, E.; Dincer, I. Magnetostructural transition in Co-Mn-Ge systems tuned by valence electron concentration. *J. Alloys Compd.* **2019**, *791*, 208-214.
- 20. Rodríguez-Carvajal, J. Recent advances in magneticstructure determination by neutron powder diffraction. *Physica B* **1993**, *192*, 55-69.
- 21. Kresse, G.; Furthmüller, J. Efficient iterative schemes for ab initio total-energy calculations using a plane-wave basis set. *Phys. Rev. B* **1996**, *54*, 11169-11186.
- 22. Kresse, G.; Joubert, D. From ultrasoft pseudopotentials to the projector augmented-wave method. *Phys. Rev. B* **1999**, *59*, 1758-1775.
- 23. Perdew, J. P.; Burke, K.; Ernzerhof, M. Generalized gradient approximation made simple. *Phys. Rev. Lett.* **1996**, *77*, 3865-3868.
- 24. Methfessel, M.; Paxton, A. T. High-precision sampling for Brillouin-zone integration in metals. *Phys. Rev. B* **1989**, *40*, 3616-3621.
- 25. Blochl, P. E.; Jepsen, O.; Andersen, O. K. Improved tetrahedron method for Brillouin-zone integrations. *Phys. Rev. B* **1994**, *49*, 16223-16233.
- Dronskowski, R.; Blochl, P. E. Crystal Orbital Hamilton Populations (COHP) - energy-resolved visualization of chemical bonding in solids based on density-functional calculations. *J. Phys. Chem.* 1993, 97, 8617-8624.
- 27. Deringer, V. L.; Tchougréeff, A. L.; Dronskowski, R. Crystal Orbital Hamilton Population (COHP) analysis as projected from plane-wave basis sets. *J. Phys. Chem. A* **2011**, *115*, 5461-5466.
- 28. Maintz, S.; Deringer, V. L.; Tchougréeff, A. L.; Dronskowski, R. LOBSTER: A tool to extract chemical bonding from planewave based DFT. *J. Comput. Chem.* **2016**, *37*, 1030-1035.
- 29. Szytuła, A.; Pędziwiatr, A. T.; Tomkowicz, Z.; Bażela, W. Crystal and magnetic structure of CoMnGe, CoFeGe, FeMnGe and NiFeGe. J. Magn. Magn. Mater. 1981, 25, 176-186.
- 30. Ener, S.; Fries, M.; Hammerath, F.; Opahle, I.; Simon, E.; Fritsch, P.; Wurmehl, S.; Zhang, H.; Gutfleisch, O. Magnetic and magnetocaloric properties of the $\text{Co}_{2-x}\text{Mn}_x\text{B}$ system by

- experiment and density functional theory. *Acta Mater.* **2019**, *165*, 270-277.
- Asada, K.; Fujita, A.; Fukamichi, K. Magnetic moment and spin-wave stiffness constant of La(Co_{1-x}Mn_x)₁₃ compounds consisting of icosahedrons. *J. Alloys Compd.* 2003, 354, 72-77.
- 32. Qian, P.; Wang, Q.-L.; Chen, N.-X.; Shen, J. Atomistic simulation for structural and vibrational properties of $R_2Co_{7-x}M_xB_3$ (R = Y, Gd; M = Ti, V, Cr). *J. Phys. D* **2006**, *39*, 1197-1203.
- 33. Karlsen, O. B.; Kjekshus, A.; Fjellvåg, H.; Ravindran, P.; Vidya, R.; Hauback, B. C. Structure and magnetism of the β-Mn–Co solid-solution phase. *J. Alloys Compd.* **2009**, *476*, 9-13.
- 34. Deringer, V. L.; Zhang, W.; Rausch, P.; Mazzarello, R.; Dronskowski, R.; Wuttig, M. A chemical link between Ge-Sb-Te and In-Sb-Te phase-change materials. *J. Mater. Chem. C* **2015**, *3*, 9519-9523.
- 35. Wuttig, M.; Lüsebrink, D.; Wamwangi, D.; Wełnic, W.; Gilleßen, M.; Dronskowski, R. The role of vacancies and local distortions in the design of new phase-change materials. *Nat. Mater.* **2007**, *6*, 122-128.
- 36. Landrum, G. A.; Dronskowski, R. Ferromagnetism in transition metals: a chemical bonding approach. *Angew. Chem. Int. Ed.* **1999**, *38*, 1390-1393.
- Landrum, G. A.; Dronskowski, R. The orbital origins of magnetism: from atoms to molecules to ferromagnetic alloys. *Angew. Chem. Int. Ed.* 2000, 39, 1560-1585.
- 38. Zhang, H.; Li, Y.; Liu, E.; Tao, K.; Wu, M.; Wang, Y.; Zhou, H.; Xue, Y.; Cheng, C.; Yan, T.; Long, K.; Long, Y. Multiple magnetic transitions in MnCo_{1-x}Cu_xGe driven by changes in atom separation and exchange interaction. *Mater. Design* **2017**, *114*, 531-536.
- 39. Liu, J.; You, Y.; Batashev, I.; Gong, Y.; You, X.; Huang, B.; Zhang, F.; Miao, X.; Xu, F.; van Dijk, N.; Brück, E. Design of reversible low-field magnetocaloric effect at room temperature in hexagonal Mn*MX* ferromagnets. *Phys. Rev. Appl.* **2020**, *13*, 054003.
- 40. Wang, J.-T.; Wang, D.-S.; Chen, C.; Nashima, O.; Kanomata, T.; Mizuseki, H.; Kawazoe, Y. Vacancy induced structural and magnetic transition in MnCo_{1-x}Ge. *Appl. Phys. Lett.* **2006**, *89*, 262504.
- 41. Johnson, V. Diffusionless orthorhombic to hexagonal transitions in ternary silicides and germanides. *Inorg. Chem.* **1975**, *14*, 1117-1120.
- 42. Gercsi, Z.; Hono, K.; Sandeman, K. G. Designed metamagnetism in CoMnGe_{1-x}P_x. *Phys. Rev. B* **2011**, *83*, 174403.
- 43. Nizioł, S.; Bombik, A.; Bazela, W.; Szytuła, A.; Fruchart, D. Crystal and magnetic structure of Co_xNi_{1-x}MnGe system. *J. Magn. Magn. Mater.* **1982**, *27*, 281-292.
- 44. Bao, L.-F.; Huang, W.-D.; Ren, Y.-J. Tuning martensitic phase transition by non-magnetic atom vacancy in MnCoGe alloys and related giant magnetocaloric effect. *Chin. Phys. Lett.* **2016**, *33*, 077502.
- 45. Law, J. Y.; Franco, V.; Moreno-Ramírez, L. M.; Conde, A.; Karpenkov, D. Y.; Radulov, I.; Skokov, K. P.; Gutfleisch, O. A quantitative criterion for determining the order of magnetic phase transitions using the magnetocaloric effect. *Nat. Commun.* 2018, 9, 2680.
- 46. Tao, K.; Zhang, H.; Long, K. W.; Wang, Y. X.; Wu, M. L.; Xiao, Y. N.; Xing, C. F.; Wang, L. C.; Long, Y. Magnetostructural transformation and large magnetocaloric effect in Mn_{0.9}Cu_{0.1}CoGe_{1-x}Si_x alloys. *Intermetallics* **2017**, *91*, 45-49.
- 47. Ren, Q. Y.; Hutchison, W. D.; Wang, J. L.; Studer, A. J.; Md Din, M. F.; Muñoz Pérez, S.; Cadogan, J. M.; Campbell, S. J. The

- magneto-structural transition in $Mn_{1-x}Fe_xCoGe$. *J. Phys. D* **2016**, 49, 175003.
- 48. Wang, G. F.; Zhao, Z. R.; Song, L.; Tegus, O. Peculiar influence of Mn/Fe ratio on the magnetic and magnetocaloric properties of $Mn_{2-x}Fe_xP_{0.6}Si_{0.25}Ge_{0.15}$ compounds. *J. Alloys Compd.* **2013**, *554*, 208-213.
- 49. Bonilla, C. M.; Herrero-Albillos, J.; Bartolomé, F.; García, L. M.; Parra-Borderías, M.; Franco, V. Universal behavior for magnetic entropy change in magnetocaloric materials: An analysis on the nature of phase transitions. *Phys. Rev. B* **2010**, *81*, 224424.

TOC Graphics

